JOURNAL OF GEOPHYSICAL RESEARCH, VOL. 115, A05213, doi:10.1029/2009JA014743, 2010

Plasma sheet thickness during a bursty bulk flow reversal

E. V. Panov,[1,2] R. Nakamura,[1] W. Baumjohann,[1] V. A. Sergeev,[3] A. A. Petrukovich,[4] V. Angelopoulos,[5] M. Volwerk,[1] A. Retinò,[1] T. Takada,[6] K.-H. Glassmeier,[7,8] J. P. McFadden,[9] and D. Larson[9]

Received 12 August 2009; revised 21 October 2009; accepted 14 December 2009; published 20 May 2010.

[1] On 17 March 2008 around 0912 UT the five THEMIS spacecraft P1–P5 were in the plasma sheet between 2200 and 2300 h magnetic local time (MLT), covering radial distances between 15 Earth radii (Re) (P1) and 9 Re (P5). All the spacecraft consecutively observed a bursty bulk flow (BBF) that traveled earthward, slowed down from 400 km/s to 50 km/s between P1 and P5, and then turned in the opposite direction. The most tailward-located spacecraft, P1 and P2, detected thinning and then thickening of the plasma sheet around the time of the flow direction change. Meanwhile, the other three THEMIS spacecraft, which were located in a more dipolar region, observed plasma sheet thickening and then thinning. Observations indicated that the thinning/thickening was stronger around the BBF funnel. Further, during the interaction of the earthward-flowing BBF plasma with the Earth's dipolar field lines, the BBF was deflected by about 70° at a scale of about 5 Re. The radial pressure gradient was substantially increased when the BBF reached the shortest radial distance to the Earth and substantially decreased after the tailward plasma flow. We conclude that the tailward pressure pulse produced by the enhanced radial pressure gradients after the earthward BBF stopped could be responsible for the observed tailward plasma flows.

Citation: Panov, E. V., et al. (2010), Plasma sheet thickness during a bursty bulk flow reversal, *J. Geophys. Res.*, *115*, A05213, doi:10.1029/2009JA014743.

1. Introduction

[2] Previous observations of the magnetotail at radial distances 13–19 Re from the Earth revealed that plasma sheet thickness can vary between 0.5 and 5 Re [*McComas et al.*, 1986; *Baumjohann and Paschmann*, 1990; *Baumjohann et al.*, 1992; *Sergeev et al.*, 1993; *Sanny et al.*, 1994; *Zhou et al.*, 1997; *Thompson et al.*, 2005; *Runov et al.*, 2005a, 2005b; *Petrukovich et al.*, 2007]. It is commonly accepted that the plasma sheet slowly thins during the substorm growth phase [*Baumjohann et al.*, 1992; *Rostoker*, 1996; *McPherron et al.*, 1987; *Lui et al.*, 1990; *Schindler and Birn*, 1993; *Birn et al.*, 1999]. It regains its initial thickness around the beginning of the recovery phase [*Baumjohann et al.*, 1992].

[3] Bursty bulk flows (BBFs), fast plasma flows inside the plasma sheet [*Hayakawa et al.*, 1982; *Baumjohann et al.*, 1989, 1990; *Angelopoulos et al.*, 1992, 1994], are often associated with substorms [*Baumjohann et al.*, 1991, 1999]. As shown by recent CLUSTER observations [*Nakamura et al.*, 2002b], the plasma sheet can also thin rapidly as a BBF propagates inside it.

[4] Multispacecraft observations have revealed that BBFs occur in very localized channels up to 2–3 Re wide [*Angelopoulos et al.*, 1996; *Sergeev et al.*, 1996; *Nakamura et al.*, 2004; *Snekvik et al.*, 2007]. At around 10 Re, BBFs are suddenly decelerated by the dominant dipolar magnetic field, and pressure gradients are piled up, leading to a substorm current wedge [*Baumjohann*, 2002].

[5] The arrival of BBFs at the inner edge of the plasma sheet leads to dipolarization of the magnetotail [*Nakamura et al.*, 1994; *Schödel et al.*, 2001a, 2001b; *Baumjohann*, 2002; *Nakamura et al.*, 2002a, 2004; *Kaufmann et al.*, 2005; *Ohtani et al.*, 2006; *Takada et al.*, 2006; *Kaufmann and Paterson*, 2008]. Dipolarization is first observed in the near-Earth plasma sheet and then moves tailward [*Baumjohann et al.*, 1999]. Dipolarization may be important for contributing to the plasma sheet population of suprathermal electrons [*Åsnes et al.*, 2008].

[6] Observations, analytical calculations, and MHD modeling [*Goertz and Baumjohann*, 1991; *Chen and Wolf*,

[1]Space Research Institute, Austrian Academy of Sciences, Graz, Austria.
[2]On leave from Space Research Institute of Russian Academy of Sciences, Moscow, Russia.
[3]Institute of Physics, Saint Petersburg State University, Saint Petersburg, Russia.
[4]Space Research Institute of Russian Academy of Sciences, Moscow, Russia.
[5]Institute of Geophysics and Planetary Physics, University of California, Los Angeles, California, USA.
[6]Institute of Space and Astronautical Science, Sagamihara, Japan.
[7]Institut für Geophysik und Extraterrestrische Physik, Technische Universität Braunschweig, Brunswick, Germany.
[8]Max Planck Institute for Solar System Research, Katlneburg-Lindau, Germany.
[9]Space Science Laboratory, University of California, Berkeley, California, USA.

0148-0227/10/2009JA014743

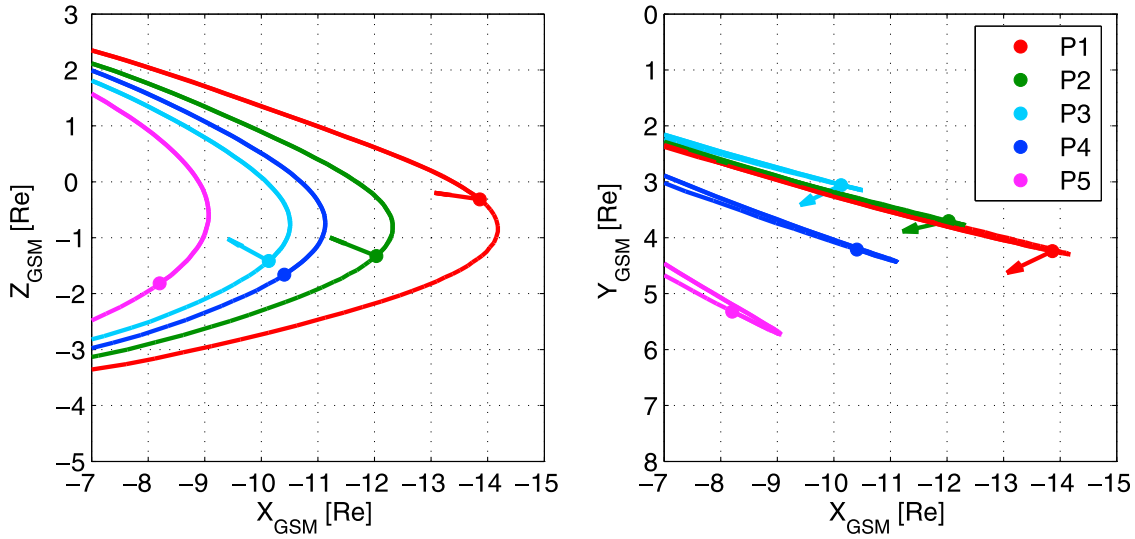

Figure 1. Location of five THEMIS spacecraft on 17 March 2007 around 0912 UT in noon (left) meridian and (right) equatorial GSM planes and the corresponding magnetic field lines according to the adapted Tsyganenko 96 model [*Tsyganenko and Stern*, 1996; *Kubyshkina et al.*, 2009]. See legend for color coding. Red, green, and cyan arrows show directions of the minimum variance of the magnetic field.

1993, 1999; *Birn et al.*, 2004] have suggested that BBFs can be thought of as thin filaments inside the plasma sheet with entropy that is substantially lower than that of the surrounding plasma, resulting in earthward acceleration by the plasma buoyancy force. *Chen and Wolf* [1999] predicted that "overshooting" may cause BBFs to bounce tailward in the near-Earth plasma sheet. This find is generally consistent with Geotail observations of tailward flows in the near-Earth plasma sheet [*Ohtani et al.*, 2009].

[7] MHD modeling results [*Birn et al.*, 1999, 2004; *Ugai*, 2009a, 2009b] have predicted that the interaction of an incident flow in the plasma sheet with dipolar field lines of the Earth's magnetic field would result in flow deflection and formation of plasma vortices. Indeed, recent THEMIS observations have indicated signatures of vortical plasma motion in the near-Earth plasma sheet [*Keiling et al.*, 2009; *Keika et al.*, 2009]. Because of the small separation between the spacecraft, however, these observations could only provide a low estimate of the possible size of the vortex: about 2 Re.

[8] With the help of measurements from five identical THEMIS spacecraft on 17 March 2007 around 0912 UT [*Angelopoulos*, 2008], we readdress the above questions. In particular, (1) we demonstrate that the passage of a BBF leads to simultaneous local plasma sheet thinning and thickening at different radial distances from the Earth, (2) we show that the size extent of the plasma vortex formed during the flow deflection can be as large as 10 Re, and (3) we investigate the process of the BBF bouncing off the Earth's dipolar magnetic field lines in more detail and indicate that substantially increased radial pressure gradients could provide a pressure pulse and accelerate plasma tailward.

2. Observations

2.1. Event Overview

[9] Figure 1 shows the locations of the five THEMIS spacecraft on 17 March 2007 at around 0912 UT in the midnight meridian (Figure 1, left) and equatorial (Figure 1, right) GSM planes. The color scheme used to denote the five spacecraft can be found in the legend. The five spacecraft, located between 2200 and 2300 MLT, covered radial distances between 15 Re and 10 Re: P1 (red) at (−13.862, 4.240, −0.314) Re, P2 (green) at (−12.030, 3.701, −1.329) Re, P3 (cyan) at (−10.129, 3.059, −1.419) Re, P4 (blue) at (−10.408, 4.212, −1.660) Re and P5 (magenta) at (−8.205, 5.320, −1.817) Re in the GSM frame of reference.

[10] We also plot the Earth's magnetic field lines calculated using an adapted Tsyganenko 96 model [*Tsyganenko and Stern*, 1996; *Kubyshkina et al.*, 2009], which predicted that magnetic field line footprints would be found at approximately 68°N and 220°W. These coordinates were covered by the Fort Yukon Ground-Based Observatory (FYKN GBO) for the study of auroral substorms. The FYKN GBO observed intense auroras between 0912 and 0919 UT just above 70°. Note that the auroral emissions have moved several degrees poleward with respect to their beginning footprint of brightening (see FYKN GBO Animation 1 or visit GBO Web-based service available at http://themis.ssl.berkeley.edu/gbo/datenav.html).[1]

[11] For our analysis we used 128 Hz resolution magnetic field data from the THEMIS fluxgate magnetometers (FGM) [*Auster et al.*, 2008] and sampled ion and electron distribution functions once every 3 seconds for particles with energies less than 30 keV from the THEMIS Electrostatic Analyzers (ESA) [*McFadden et al.*, 2008] and from Solid State Telescopes (SST) for particles with energies more than 30 keV. We used the combined ESA and SST ion moments to improve the quality of the ion data.

[12] Figure 2 shows data from the five THEMIS spacecraft during the BBF event. They are plotted, from top to bottom, in the sequence of the BBF encounter by the spacecraft: P1, P2, P4, P3, and P5. Figure 2 (top) shows 3 s

[1] Animations 1 and 2 are available in the HTML.

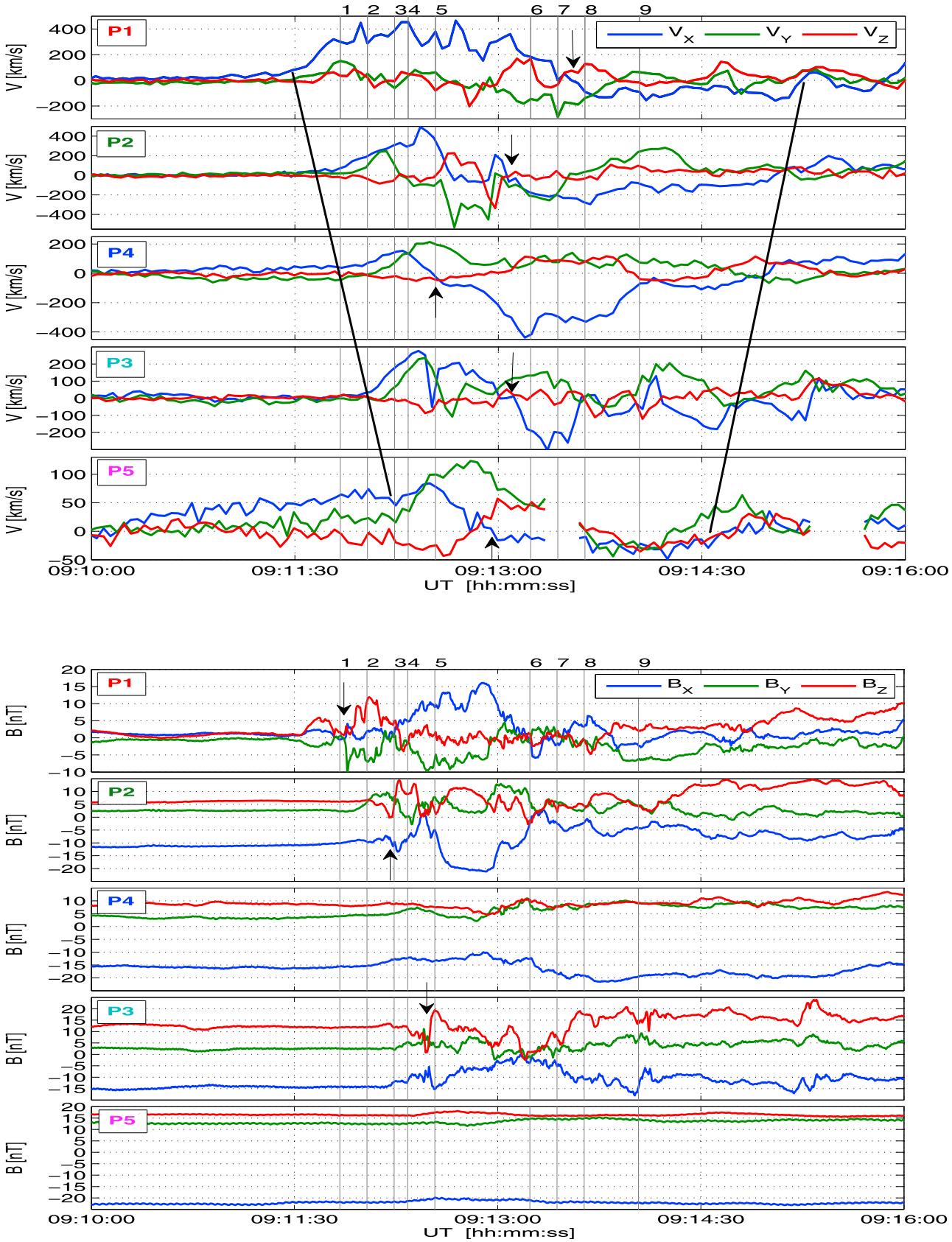

Figure 2. (top) Velocity and (bottom) magnetic field GSM components from five THEMIS spacecraft on 17 March 2007 between 0910 and 0916 UT. See legends for color coding.

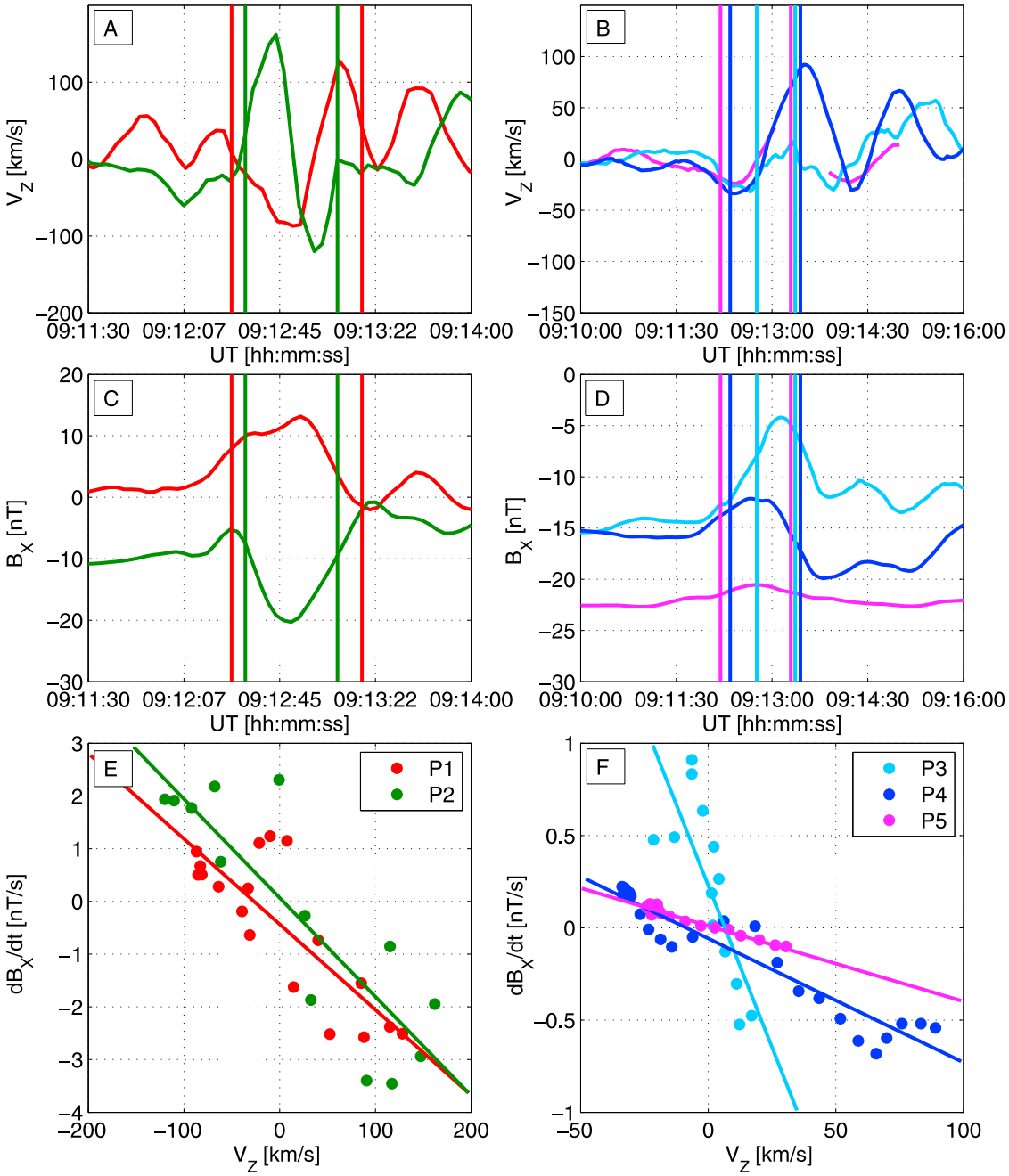

Figure 3. (a and b) The GSM V_Z component of the plasma bulk velocity, (c and d) GSM B_X component of the magnetic field, dependence of the B_X time derivative dB_X/dt on V_Z, and (e and f) the corresponding linear best fits for five THEMIS spacecraft on 17 March 2007. The vertical lines in Figures 3a–3d delimit the time intervals used for plotting Figures 3e and 3f. See legend for color coding.

(spin) resolution GSM components of the ion bulk velocity; Figure 2 (bottom) shows 128 Hz sampled GSM components of the magnetic field (see legends for color coding). The left thick black line in Figure 2 indicates BBF onset for the five spacecraft.

[13] Further, the X component of the velocity changed toward negative values at all five spacecraft as indicated by black arrows in the plasma velocity part of Figure 2. The tailward flow continued until the second thick black line. As one can see, the five spacecraft met the end of the tailward flow in an inverted sequence.

[14] In Figure 2 (bottom), one can see that the three spacecraft (P1, P2, and P3) observed strong magnetic field fluctuations. Less clear were magnetic field fluctuations observed by P4 and P5. As shown in Figure 1, P1, P2, and P3 were located at nearly the same MLT, whereas P4 and P5 were up to 1 h MLT duskward from the other spacecraft. Such observations suggest that the bulk flows were localized in the azimuthal direction within the distance between the spacecraft, i.e., within several Re.

[15] From P1, P2, and P3 magnetic field observations, one can identify a magnetic boundary of the observed BBF

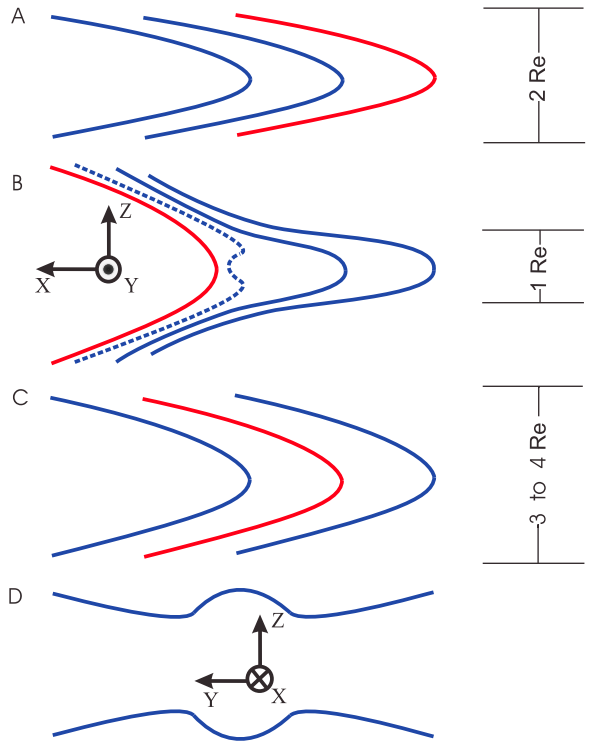

Figure 4. A sketch showing the plasma sheet magnetic field lines in the (X, Z) GSM plane (a) before, (b) during, and (c) after BBF passage. During BBF passage the left side of the plasma sheet thickened and its right side thinned from 2 Re to 1 Re. The same magnetic field line is shown in red. After the BBF passed, the plasma sheet dipolarized, becoming between 3 and 4 Re thick, i.e., 1.5–2 times thicker than before BBF arrival. The dashed field line is bent earthward closer to the central plasma sheet (see section 3 for details). (d) We also show a possible cross-tail slice of the earthward part of the plasma sheet as BBF propagates inside it.

[*Sergeev et al.*, 1996]. We indicated this boundary by the black arrows in the magnetic field part of Figure 2. With the help of minimum variance analysis, we derived the orientation **N** of the observed magnetic boundaries and show the normal vectors to them in Figure 1 with red arrows for P1, $\mathbf{N}_1$ = (0.89; 0.43; 0.13); green arrows for P2, $\mathbf{N}_2$ = (0.91; 0.21; 0.37); cyan arrows for P3, $\mathbf{N}_3$ = (0.80; 0.40; 0.44). All vectors point in a similar direction in the (X, Y) GSM plane at an angle to the X axis around 15° duskward. The timing between these three spacecraft provided the propagation velocity of the boundary from P1 to P2 and then to P3 of about V = 725 ± 25 km/s. This value is close to the Alfvén velocity in the plasma sheet boundary layer (PSBL), assuming a magnetic field of 20 nT and a density of about 0.05–0.1 cm^{-3}, as observed by P1 and P2 at around 0912:45 UT.

[16] The time duration of the magnetic field gradient across the boundary on P1, P2, and P3 (not shown here) was about two seconds at all three spacecraft. Multiplying the propagating velocity V = 725 km/s by the time duration of the magnetic boundary, we found that the thickness of the BBF boundary was on the order of 1.5 × 10^3 km. This is about six proton gyroradii ρ_p in the PSBL, where the temperature was about 1 keV and the magnetic field strength about 20 nT, i.e., $\rho_p \approx$ 250 km.

2.2. Plasma Sheet Thickness During the BBF

[17] The B_X component of the magnetic field is commonly used as a proxy for the position of a spacecraft inside a horizontally oriented plasma sheet. During plasma sheet vertical motion, such as flapping [*Sergeev et al.*, 1998; *Runov et al.*, 2009] or thinning/thickening [*Nakamura et al.*, 2002b], the time derivative of B_X should depend on the vertical plasma velocity V_Z [*Bowling and Russell*, 1976; *Sergeev et al.*, 1993, 1998; *Petrukovich et al.*, 2003]. With the help of Figure 3, we investigate the vertical motion of the plasma sheet during passage of the BBF. Figure 3 (left) shows P1 (red) and P2 (green) data from 0911:30 to 0914 UT, and Figure 3 (right) shows P3 (cyan), P4 (blue), and P5 (magenta) data from 0910 to 0916 UT on 17 March 2007 (the vertical motion detected by P1 and P2 occurred on a shorter time interval). The Z_{GSM} component of the plasma bulk velocity (V_Z) and the X_{GSM} component of the magnetic field (B_X) are shown in Figure 3 (top) and Figure 3 (middle), respectively. For the sake of better visibility we filtered out fluctuations with time periods shorter than 15 seconds in both B_X and V_Z data.

[18] The time intervals delimited by vertical lines in Figures 3a–3d were chosen around one-period wave signatures in the V_Z components. Figures 3e and 3f show dependence of the time derivative dB_X/dt on V_Z for the time intervals delimited by the vertical lines. One can see that all five spacecraft demonstrated negative correlations between dB_X/dt and V_Z.

[19] According to the signs of B_X, P1 and P2 were located on different sides of the central plasma sheet. Figure 3a shows that at around 0912:45 UT, P1 and P2 reached the maximum in $|B_X|$ in opposite hemispheres. Hence, the plasma sheet was thinning before 0912:45 UT and then thickening until 0913:20 UT. The vertical distance between P1 and P2 was about 1 Re. From different plasma sheet parameters, such as Alfvén velocity, plotted for all five spacecraft against B_X (not shown here), one can determine that the PSBL magnetic field was about 20 nT. Hence, before BBF arrival, P1 and P2 were located away from the center of the plasma sheet by approximately one fourth of its thickness. This provides us with an estimate of plasma sheet thickness before BBF arrival of about 2 Re, which corresponds to 50 ρ_p in PSBL, where ρ_p is the thermal proton gyroradius.

[20] During the BBF, spacecraft P1 and P2 observed magnetic fields close to those in PSBL (20 nT). This means that the plasma sheet thinned to about half its previous thickness, from 2 to 1 Re (or to 25 ρ_p in PSBL). We note that since the distance along the X axis between P1 and P2 was comparable to the plasma sheet thickness, another interpretation of the vertical motion of the near-Earth plasma sheet, like, e.g., twisting seems to be unlikely. In the magnetic field data from P1 and P2 in Figure 2 after 0914 UT (after the BBF), one can also find greater B_Z and smaller B_X than before the thinning/thickening. Hence, the final plasma sheet was thicker than the initial one. Taking the PSBL magnetic field equal $B_0 = 20nT$, and noticing that B_X changed from 10 nT to 5–7 nT (P2 B_X in Figure 2 before and after BBF), we can estimate that the thickness

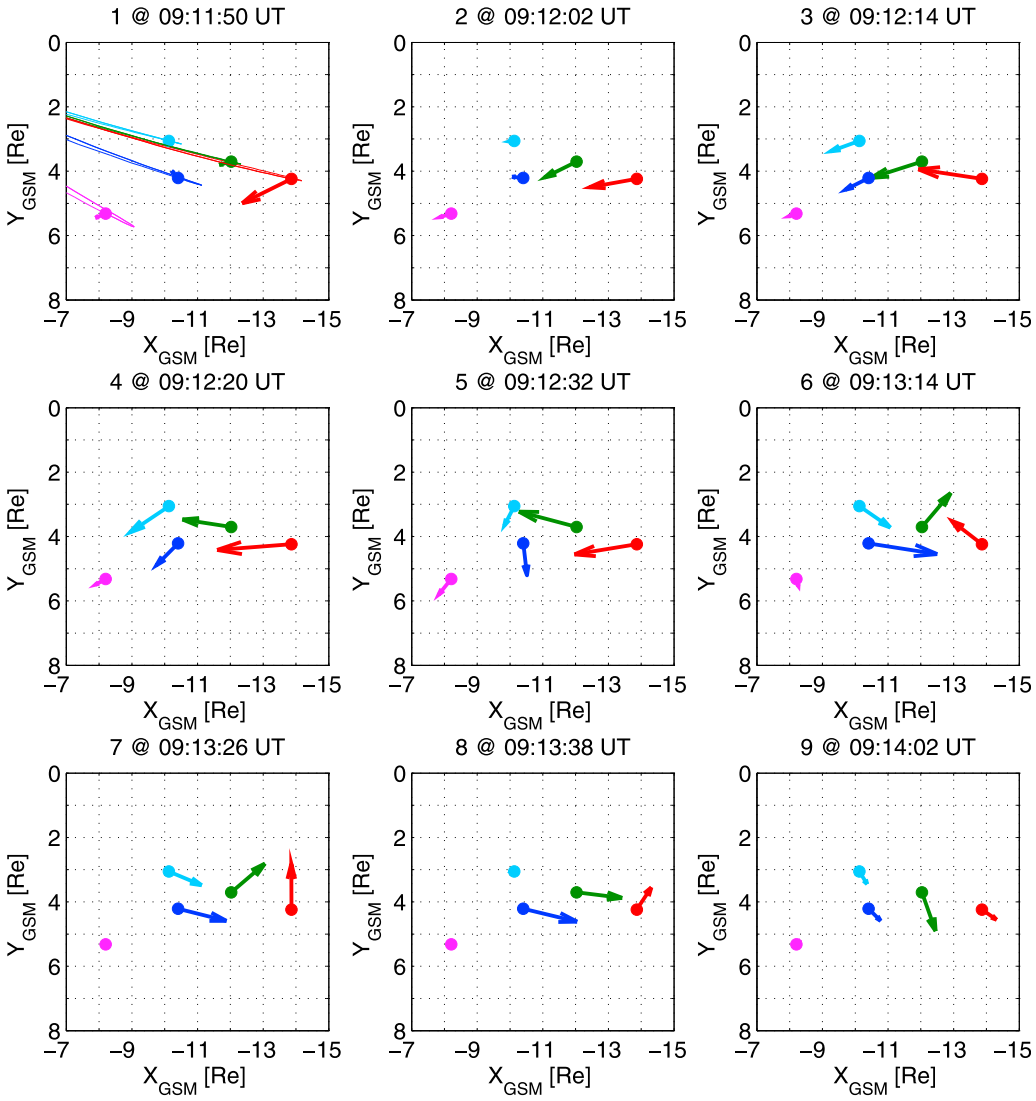

Figure 5. Selected sequential snapshots of the plasma velocity field in the (X, Y) GSM plane inside a plasma sheet during BBF passage as observed by five THEMIS spacecraft. The snapshots are numbered from left to right and from top to bottom. Times are shown above the snapshots and marked as in Figure 2 by grey vertical lines. The corresponding magnetic field lines are overplotted in accordance with the adapted Tsyganenko 96 model [*Tsyganenko and Stern*, 1996; *Kubyshkina et al.*, 2009]. See also Animation 2 containing all the snapshots.

of the current sheet, assuming a Harris current sheet profile $B_X(Z) = B_0\tanh(Z - Z_0/L_B)$, where L_B is the current sheet thickness [*Harris*, 1962]. We find that the thickness of the dipolarized plasma sheet after the BBF (after about 0914 UT) appeared to be between 3 and 4 Re.

[21] The other three spacecraft, P3, P4, and P5, were located closer to the Earth and farther from the central plasma sheet. Figure 3 shows that their B_X and V_Z profiles look similar to the observations of P1. P3, P4, and P5 were located southward of the central plasma sheet, however. Hence, contrary to the observations of P1 and P2, the data from P3, P4, and P5 indicate that the plasma sheet first thickened and then thinned. As one can see, the rate of thinning/thickening detected by P3 is close to that observed by P1 and P2. Also, the rates of thinning/thickening detected by P4 and P5 are lower than those at P1 and P2. For example, for P5 $dB_X/dt(V_Z) \approx 2 \times 10^{-3} nT/s$ and for P4 dB_X/dt $(V_Z) \approx 10^{-2} nT/s$. The different rates at P5 (smallest), P4 (intermediate), and P3 (largest) imply that a stronger thinning/thickening of the plasma sheet was observed at P3. This fact agrees with the previously made suggestion that the bursty bulk flow plasma was moving inside a narrow funnel whose axis in the (X, Y) GSM plane was close to the MLT of the P1, P2, and P3 spacecraft.

[22] Figure 4 summarizes the results of the analysis presented in Figure 3. Figure 4a illustrates the magnetic field lines in the plasma sheet before BBF arrival, when the plasma sheet thickness was about 2 Re. Figure 4b demonstrates the thinning of the tailward (right) part of the plasma sheet and the thickening of its earthward (left) part. The tailward part of the plasma sheet, observed by P1 and P2, reached a thickness of 1 Re. At the same time, data from P3,

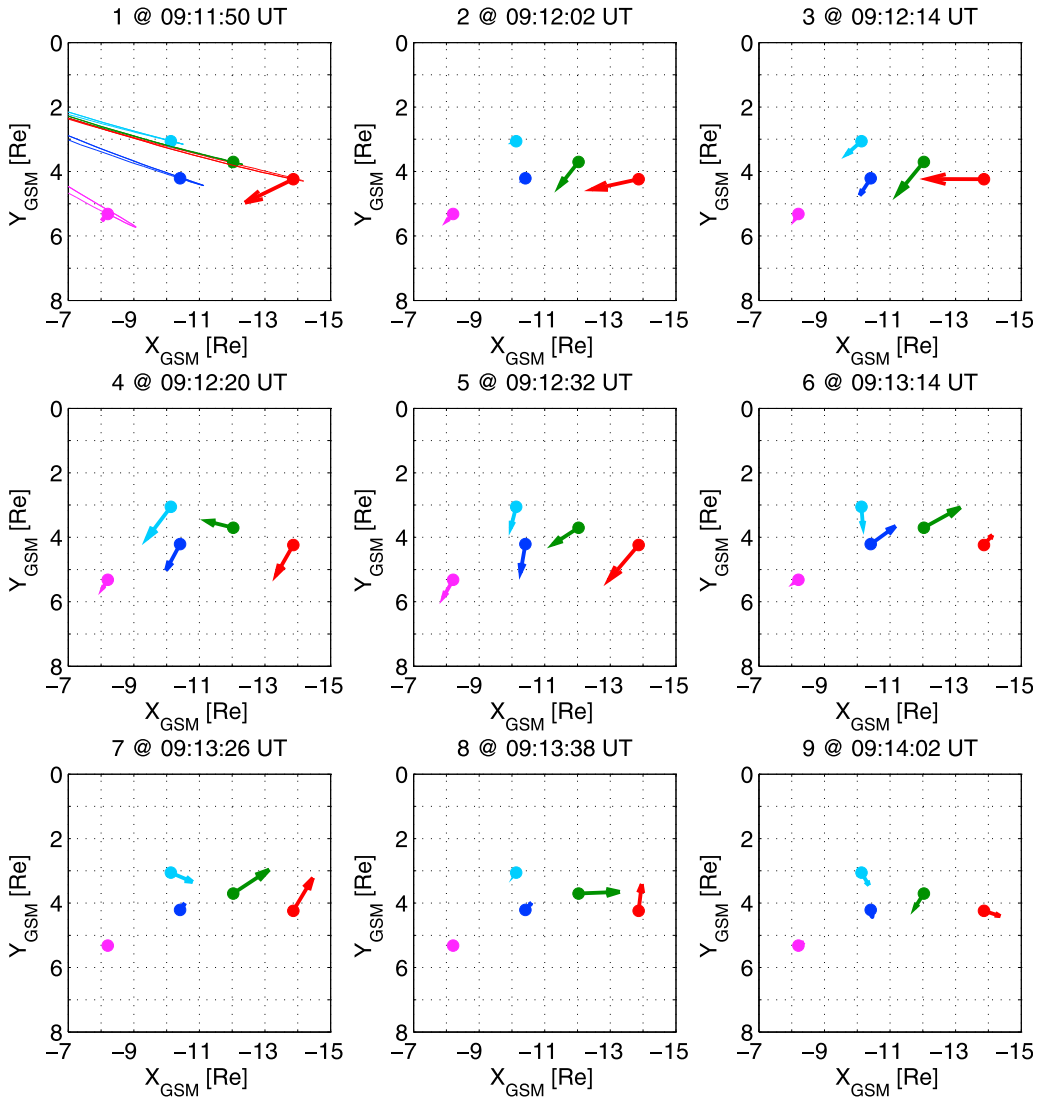

Figure 6. Same as in Figure 5 but for the velocity component perpendicular to the local magnetic field.

P4, and P5 indicated that the plasma sheet thickened. Because P3, P4, and P5 were located below the central plasma sheet, we were unable to estimate plasma sheet thickness at their locations. In Figure 4c we sketch the plasma sheet after BBF passage. Its tailward (right) part thickened and its earthward part (left) thinned. The final plasma sheet thickness appeared to be about 3 to 4 Re. In Figure 4d we plot a possible cross-tail slice of the earthward part of the plasma sheet during BBF passage. The near-Earth magnetotail plasma sheet, which is typically thinner at the midnight meridian [*Tsyganenko and Mukai*, 2003; *Birn*, 2005], is locally thickened as BBF propagates inside it.

2.3. Deflection of the BBF

[23] Figure 5 shows selected sequential snapshots of the plasma velocity field in the (X, Y) GSM plane inside the plasma sheet as observed by THEMIS between 0911:50 and 0914:02 UT. The snapshots are numbered at the top. The initial configuration of the magnetic field lines, as predicted by the adapted Tsyganenko 96 model [*Tsyganenko and Stern*, 1996; *Kubyshkina et al.*, 2009], is shown in the first snapshot. The three top snapshots show how the BBF arrived at P1 at 0911:50 UT, at P2 at 0912:02 UT, and finally at P3 and P4 at 0912:14 UT.

[24] At the moment of arrival, the plasma velocity was oriented in approximately the same direction as the normals to the BBF magnetic boundaries, shown by red, green and cyan vectors in Figure 1. In the fourth snapshot of Figure 5 at 0912:20 UT, one can recognize a deflection pattern in the plasma flow: earthward-flowing plasma at P1 and P2 changed direction to duskward at P5, P3, and P4. Plasma flow deflection of about 70° occurred along a path with a curvature radius of approximately 5 Re.

[25] The following four snapshots, between 0912:38 UT and 0913:38 UT, show that the plasma flow changed direction further tailward. The direction change was observed through the dusk side by P4 and P5 and through the dawn side by P1 and P2. Finally, at 0914:02 the plasma appeared to flow tailward and duskward, as detected by P1, P2, P3, and P4.

[26] In order to clarify the motion of the magnetic flux with respect to these plasma flows, we show the convective

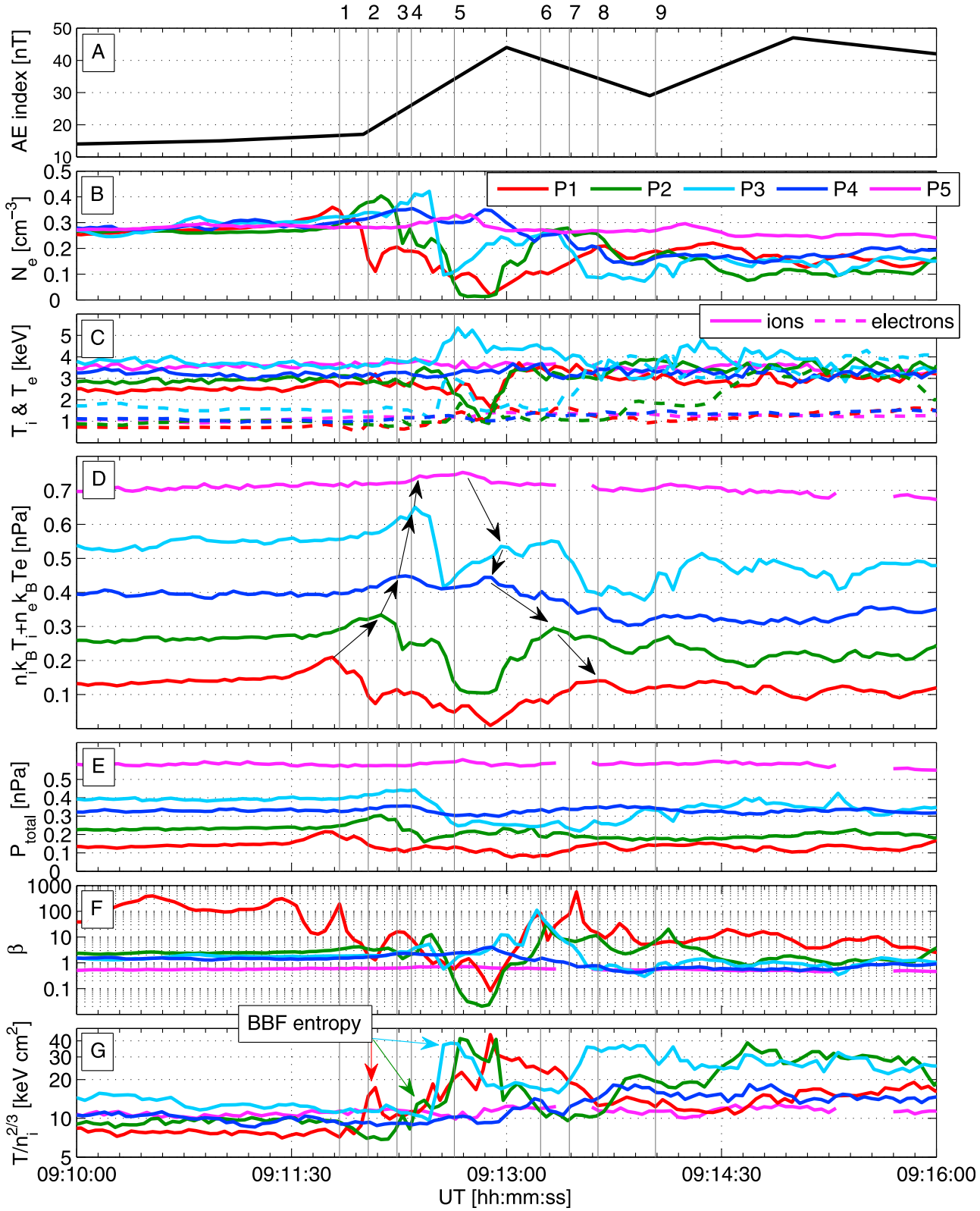

Figure 7. *AE* index and data from five THEMIS spacecraft on 17 March 2007 between 0910 and 0916 UT: (a) electron density, (b) ion temperature (solid lines), (c) electron temperature (dashed lines), (d) plasma pressure $n_i k_B T_i + n_e k_B T_e$ (for better visibility we shifted the traces for P2 by 0.1 nPa, for P3 by 0.3 nPa, for P4 by 0.2 nPa and for P5 by 0.5 nPa, the black arrows show the sequence of plasma pressure change during the earthward and the tailward BBF motion), (e) sum of plasma and magnetic pressure, (f) plasma $\beta = 2\mu_0(n_i k_B T_i + n_e k_B T_e)/B^2$, and (g) value of $T/n_i^{2/3}$. The color coding is the same as in Figure 1.

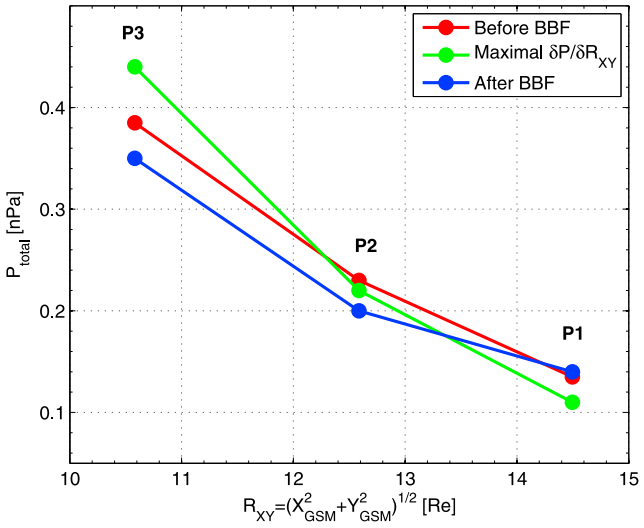

Figure 8. Changes in total pressure before (at 0910 UT, in red), during (at the time of the maximum spatial pressure gradient $\bigtriangledown p_r$ at 0912:20 UT, in green), and after (at 0916 UT, in blue) the bursty bulk flow on 17 March 2008, as observed by P1, P2, and P3.

(perpendicular) part of the flow velocity in Figure 6 in the same layout as in Figure 5. By comparing snapshots 5 through 9 in Figures 5 and 6, one can see that the rotation of the plasma flow at P4 and P5 largely included plasma flow parallel to the magnetic field. The rotation of the plasma flow, observed by P1 and P2 was mainly perpendicular, i.e., accompanied by motion of the corresponding magnetic flux tubes. We sketched this in Figure 4, where the same magnetic field line is shown in red. First, the magnetic flux was transported earthward together with the plasma flow; the red line moved left in Figure 4b. Then, owing to the bouncing of the plasma flow tailward, the associated magnetic flux moved tailward, as well; the red line moved right in Figure 4c. Because the final thickness of the plasma sheet appeared to be larger than before BBF arrival, however, we concluded that the tailward motion of the magnetic flux tubes would not reach its original position, which is shown in Figure 4a.

2.4. Radial Pressure Evolution

[27] Figure 7 shows changes in pressure components at the locations of the five spacecraft on 17 March 2007 between 0910 and 0916 UT. Figure 7a depicts the *AE* index. The enhancement in the *AE* index after 0912 UT suggests that the auroral electrojet was present and the substorm was at the beginning of expansion phase. The *AE* index increased constantly until about 0926 UT when it has reached a value of 130 nT (not shown here). Since the ESA detector did not provide full coverage of ion energies in the plasma sheet, we present the electron density in Figure 7b. The sum of the ion density from ESA and SST spectrometers (not shown here) was in good agreement with the electron density.

[28] The electron temperature (shown by dashed lines, Figure 7c) was about 2–2.5 times lower than the ion temperature (solid lines, Figure 7c). The ion-to-electron temperature ratio was substantially smaller than an average for a plasma sheet ($\langle T_i/T_e \rangle \approx 7$), which was estimated using AMPTE measurements [*Baumjohann et al.*, 1989, 1991; *Baumjohann*, 1993]. The electron temperature detected onboard P2 and P3 appeared to be higher after BBF passage, thus providing an input into the plasma pressure equal to that of the ions.

[29] The sum of the ion and the electron components of the plasma pressure is shown in Figure 7d. For better visibility, we shifted the traces for P2 by 0.1 nPa, for P3 by 0.3 nPa, for P4 by 0.2 nPa, and for P5 by 0.5 nPa. The arrows in Figure 7d correspond to the maxima in the plasma pressure. With the help of the upward arrows, one can follow the earthward propagation of the BBF from P1 to P5. The downward arrows indicate the times when a tailward-moving pressure maximum was observed; the spacecraft (except P3) met the pressure maximum in an inverted sequence. The tailward sequence of the plasma pressure maximum happened similarly to the sequence of the times when the flow turned tailward, as shown by the black arrows in Figure 2 (top). In Figure 7e the sum of the plasma and the magnetic pressure is depicted. One can see (mainly from P1, P2, and P3 at the same MLT) that the total pressure maximum moves earthward.

[30] In order to clarify the location of the THEMIS spacecraft with respect to the central plasma sheet we provide the plasma β profiles in Figure 7f. Figure 7g shows the value of $T_i/n_i^{2/3}$, which serves as a proxy for the local entropy. Here we use the polytropic index $\gamma = 5/3$, although in the quiet plasma sheet the polytropic index may be as small as 4/3 [*Baumjohann and Paschmann*, 1989; *Spence and Kivelson*, 1990; *Goertz and Baumjohann*, 1991]. One can see that the value of $T_i/n_i^{2/3}$ increased substantially during the BBF at the positions of P1, P2 and P3, and at the times denoted by the black vertical lines 2, 4, and 5, respectively, in Figure 7 (also highlighted by red, green, and cyan arrows). The value of $T_i/n_i^{2/3}$, however, remained nearly unchanged at the positions of P4 and P5. The latter observations indicate that the BBF developed as a thin (less than several Re) filament inside the plasma sheet. A more drastic change in the value of $T_i/n_i^{2/3}$ was found by P1 and P2 around 0913 UT, the plasma sheet thinning and thickening time (compare with P1 (red) and P2 (green) profiles of plasma β in Figure 7f).

[31] Figure 8 shows the sum of the plasma and the magnetic field pressure $n_i k_B T_i + n_e k_B T_e + B^2/2\mu_0$ versus the radial distance in the (X, Y) GSM plane $R_{XY} = (X^2 + Y^2)^{1/2}$ for P1, P2, and P3. The total pressure is shown for four times: before BBF arrival at 0910 UT (red), at the maximum spatial pressure gradient $\bigtriangledown p_r$ at about 0912:20 UT (green), and after the BBF bounced tailward and stopped, at 0916 UT (blue). When the BBF reached the shortest radial distance to the Earth, P3 observed a substantial (about 0.06 nPa) increase in the total pressure, while P1 observed a less drastic decrease (about 0.03 nPa). After the BBF bounced tailward, P3 observed a substantially stronger (0.09 nPa) pressure decrease, while the total pressure at the position of P1 returned to the initial value. As one can see in Figure 7e, the pressure changes at other MLT, as observed by P5 and P4, were much smaller.

3. Discussion

[32] If interpreted as thin filaments inside the plasma sheet with an entropy substantially different from that of the

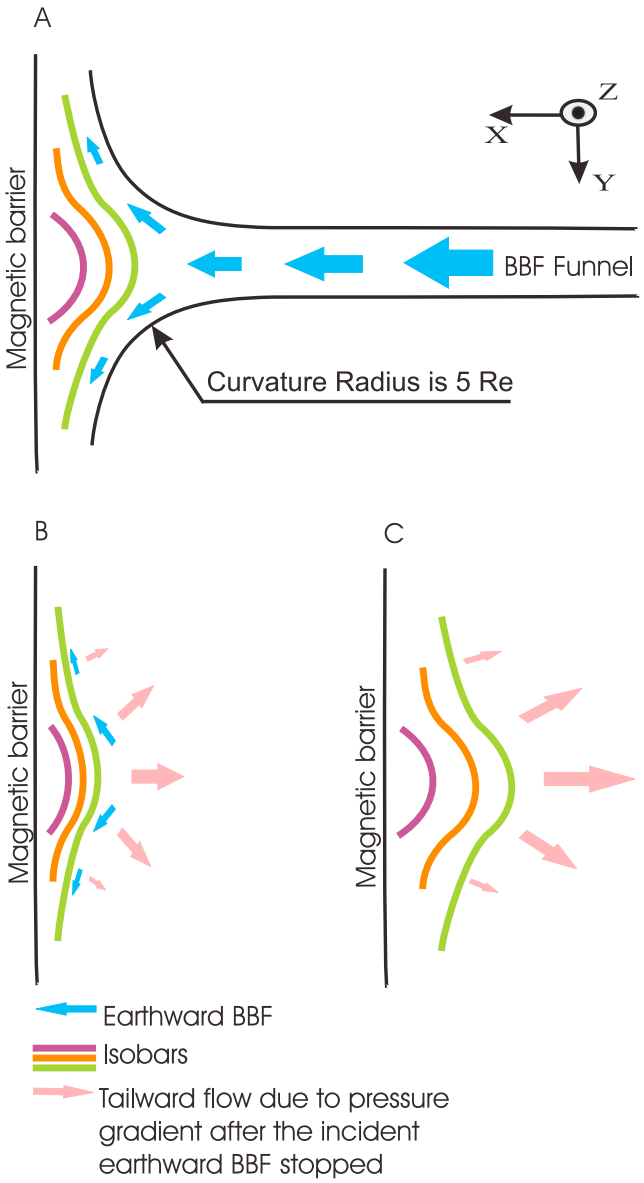

Figure 9. A sketch illustrating in (X, Y) GSM plane (a) the interaction of the earthward-moving BBF with a magnetospheric barrier, (b) consequent stopping of the earthward BBF and starting of tailward flows due to radial pressure gradients, and (c) smoothing of the pressure gradients over larger scales tailward.

surrounding plasma, BBFs are expected to be dragged earthward by the plasma buoyancy force [*Goertz and Baumjohann*, 1991; *Chen and Wolf*, 1993, 1999; *Birn et al.*, 2004]. The earthward propagation velocity of the magnetic flux at the front of the BBF, which appeared to be on the order of the Alfvén velocity in the ambient PSBL plasma, was more than two times higher than that of the fastest bursts. Thus, the magnetic field pulsations at the footprints of the magnetic field lines connected to the BBF would start much earlier than expected based on lower plasma flow velocities.

[33] The fast motion of bursty bulk flows causes changes in plasma sheet thickness [*Nakamura et al.*, 2002b]. In this paper we demonstrate that during a BBF, the plasma sheet simultaneously thins and thickens at different radial distances from the Earth. The thinning/thickening appears to be stronger at the center of the BBF funnel. The stage of the plasma sheet reflected in Figure 4b, based only on spacecraft observations, is in a remarkable agreement with the evolution of magnetic field lines shown by MHD simulations [*Birn et al.*, 1999; *Ugai*, 2009a, 2009b]. For instance, in Figure 3 of *Birn et al.* [1999] one can recognize both plasma sheet thinning tailward from 10 Re and a small thickening earthward from 10 Re.

[34] The interaction of the earthward-moving BBF with the more dipolar field lines at 7–10 Re resulted in flow deflection. The vortical plasma motion formed at a scale of 10 Re, in agreement with global MHD modeling estimates [*Birn et al.*, 1999; *El-Alaoui*, 2001; *Birn et al.*, 2004; *Ugai*, 2009a, 2009b; *El-Alaoui et al.*, 2009] and much larger than the estimates of *Keika et al.* [2009] and *Keiling et al.* [2009]. A larger study is needed for understanding the statistical characteristics of the vortices. The modeling and observations also indicated formation of strong parallel currents by plasma vortices [*Keiling et al.*, 2009]. These currents produce auroral emissions. The FYKN GBO, indeed, detected intense auroras just above 70°N between 0912 and 0919 UT. The auroral emissions from the spacecraft observations disappeared shortly after the end of the BBF.

[35] Recent MHD simulations by *Ugai* [2009a, 2009b] have also confirmed the BBF overshooting predicted by *Chen and Wolf* [1999]. Such overshooting would change the sign of the $[\mathbf{j} \times \mathbf{B}]_r$ term in the equation of motion. In situ observations of the overshooting would appear as a change of sign in the B_X component of the magnetic field, which would be stronger in the central plasma sheet. Indeed, Figure 2 shows that at around 0913:22 UT (between vertical lines 6 and 7), the B_X values observed by P2 were larger than those observed by P1: at that moment, the B_X values at P1 decreased to about −5 nT, while those at P2 increased to about 3 nT. In order to explain this as plasma sheet flapping, one must assume that the plasma sheet should have been bent northward by about 40° just within about two Earth radii, between P2 and P3, and during only several seconds. Such a strong, fast bending of the plasma sheet seems to be unrealistic, however. A more plausible explanation is local earthward bending of the magnetic field lines in the central plasma sheet, as shown by the dashed line in Figure 4b. From the magnetic field data in Figure 2, earthward bending of the magnetic field lines is expected to occur somewhere between the thinner and thicker parts of the plasma sheet.

[36] Our analysis also reveals that the pressure gradient ∇p_r was substantially increased throughout the BBF funnel when the BBF reached the shortest radial distance to the Earth. This result agrees with known radial pressure profiles around BBF onset [*Kistler et al.*, 1992]. Both the magnetic tension forces owing to BBF overshooting and the increased pressure gradient became unbalanced after the earthward kinetic pressure supplied by the plasma flows from the BBF funnel ceased. The resulting pressure pulse would push the plasma sheet ions in all directions at a velocity that can be estimated from the equation of motion $V_i = \sqrt{(\nabla p_r + [\mathbf{j} \times \mathbf{B}]_r)/2m_i n_i}$. This velocity could be as large as hundreds of kilometers per second. Note that when assuming the highest possible current density $j = \mu_0^{-1}\Delta B/L_B = 5nA/m^2$

and the value of $B_Z = 2nT$, the $[\mathbf{j} \times \mathbf{B}]_r$ term and the $\bigtriangledown p_r$ term may be equally important.

[37] Figure 9 summarizes our results regarding BBF motion in the equatorial plane. Figure 9a illustrates the interaction of the earthward-moving BBF with a magnetospheric barrier through a narrow funnel. The function of the magnetic barrier was provided by the more dipolar magnetic field lines of the Earth at $X > -10$ *Re*. The incident BBF plasma from the funnel, shown by blue arrows, was deflected by the magnetic barrier. This corresponds to the fourth snapshot in Figures 5 and 6 at 0912:20 UT. During this process the pressure gradients in front of the BBF funnel increased.

[38] Figure 9b shows the moment that corresponds to the end of the earthward BBF flow from the BBF funnel and the start of the tailward flow in the fifth snapshot in Figures 5 and 6 at 0912:32 UT. At this moment the plasma gradients in front of the BBF funnel are no longer balanced by the earthward BBF kinetic pressure. The excess in the pressure gradients pushed tailward the surrounding plasma (pink arrows), and the BBF plasma, which was still moving duskward and dawnward (blue arrows). Finally, Figure 9c shows the moment reflected in snapshot 9 in Figures 5 and 6, when the tailward motion of the pushed plasma relaxed the pressure gradients.

[39] The BBF plasma can be distinguished from the ambient plasma with the help of the entropy observations in Figure 7g. For instance, the BBF passed through P1, P2 and P3, but at P4 and P5, we probably measured the local plasma that participated in the BBF-induced circulation via pressure gradients.

[40] Recently the origin of the tailward plasma flows in the near-Earth plasma sheet was studied using multispacecraft observations. Tailward flows generated by vorticity were studied by *Keiling et al.* [2009], *Keika et al.* [2009], and *Walsh et al.* [2009]. A statistical analysis of the tailward plasma flows was performed by *Ohtani et al.* [2009], who suggested that the flows could originate from mirroring, but did not reveal the details of the mirroring and considered only the convective part of the flow velocity. Our study demonstrates that away from the BBF funnel, parallel tailward flows can be even faster than convective ones. In addition, the tailward flows need not necessarily consist of incident BBF plasma. Instead, as indicated by the entropy observations, the tailward flows detected by P4 were probably surrounding plasma pushed tailward by pressure gradients and magnetic tension forces.

[41] We note that the tailward flow formation scenario suggested in Figure 9 would destroy the vortices, and the parallel currents would stop. Therefore, our results may be important for understanding how auroral emissions terminate.

4. Conclusions

[42] Using plasma and magnetic field data from the five THEMIS spacecraft on 17 March 2008 around 0912 UT, we investigated plasma sheet dynamics during bursty bulk flows:

[43] 1. We found that all the spacecraft consecutively observed the BBF traveling earthward, slowing down from 400 km/s to 50 km/s between 15 Re and 9 Re, and then turning in the opposite direction. Timing analysis revealed that the earthward-propagating velocity of the BBF was the Alfvén velocity near the edge of the plasma sheet. The major flow burst was associated with the field lines at about the same MLT, i.e., within a BBF funnel.

[44] 2. We showed that between 15 and 13 Re the two spacecraft detected first thinning and then thickening of the plasma sheet around the time of the flow direction change. Meanwhile, in a more dipolar region (between 9 and 11 Re) the other three spacecraft indicated first plasma sheet thickening and then thinning. In addition, the observations indicated stronger thinning/thickening closer to the middle of the BBF funnel.

[45] 3. We also found that during interaction of the earthward-flowing plasma from a BBF funnel with the Earth's dipolar field lines, the BBF was deflected by about 70° at a scale of about 5 Re. In other words, the area of vortical plasma motion, where parallel currents are expected to be generated because of twisting of the magnetic field lines, was on the order of 300 Re^2.

[46] 4. We revealed that after the earthward BBF stopped, a tailward pressure pulse was produced by the enhanced radial pressure gradients, which could be responsible for the observed tailward plasma flows.

[47] **Acknowledgments.** We acknowledge NASA contract NAS5-02099 for use of data from the THEMIS mission. Specifically, U. Auster for the use of FGM data provided under the lead of the Technical University of Braunschweig and with financial support through the German Ministry for Economy and Technology and the German Center for Aviation and Space (DLR) under contract 50 OC 0302, C. W. Carlson for use of ESA data, and R. P. Lin for use of SST data. We also highly appreciate discussions with M. Fujimoto.

[48] Amitava Bhattacharjee thanks Jin-Bin Cao and another reviewer for their assistance in evaluating this paper.

References

Angelopoulos, V. (2008), The THEMIS mission, *Space Sci. Rev.*, *141*, 5–34, doi:10.1007/s11214-008-9336-1.

Angelopoulos, V., W. Baumjohann, C. F. Kennel, F. V. Coronti, M. G. Kivelson, R. Pellat, R. J. Walker, H. Luehr, and G. Paschmann (1992), Bursty bulk flows in the inner central plasma sheet, *J. Geophys. Res.*, *97*, 4027–4039.

Angelopoulos, V., et al. (1994), Statistical characteristics of bursty bulk flow events, *J. Geophys. Res.*, *99*, 21,257–21,280.

Angelopoulos, V., et al. (1996), Multipoint analysis of a bursty bulk flow event on April 11, 1985, *J. Geophys. Res.*, *101*, 4967–4990, doi:10.1029/95JA02722.

Åsnes, A., R. W. H. Friedel, B. Lavraud, G. D. Reeves, M. G. G. T. Taylor, and P. Daly (2008), Statistical properties of tail plasma sheet electrons above 40 keV, *J. Geophys. Res.*, *113*, A03202, doi:10.1029/2007JA012502.

Auster, H. U., et al. (2008), The THEMIS fluxgate magnetometer, *Space Sci. Rev.*, *141*, 235–264, doi:10.1007/s11214-008-9365-9.

Baumjohann, W. (1993), The near-Earth plasma sheet: An AMPTE/IRM perspective, *Space Sci. Rev.*, *64*, 141–163, doi:10.1007/BF00819660.

Baumjohann, W. (2002), Modes of convection in the magnetotail, *Phys. Plasmas*, *9*, 3665–3667, doi:10.1063/1.1499116.

Baumjohann, W., and G. Paschmann (1989), Determination of the polytropic index in the plasma sheet, *Geophys. Res. Lett.*, *16*, 295–298, doi:10.1029/GL016i004p00295.

Baumjohann, W., and G. Paschmann (1990), Geometry of the near-Earth plasma sheet, *J. Geophys. Res.*, *95*, 10,707–10,710, doi:10.1029/JA095iA07p10707.

Baumjohann, W., G. Paschmann, and C. A. Cattell (1989), Average plasma properties in the central plasma sheet, *J. Geophys. Res.*, *94*, 6597–6606.

Baumjohann, W., G. Paschmann, and H. Luehr (1990), Characteristics of high-speed ion flows in the plasma sheet, *J. Geophys. Res.*, *95*, 3801–3809.

Baumjohann, W., G. Paschmann, T. Hagai, and H. Luehr (1991), Superposed epoch analysis of the substorm plasma sheet, *J. Geophys. Res.*, *96*, 11,605–11,608, doi:10.1029/91JA00775.

Baumjohann, W., G. Paschmann, and T. Nagai (1992), Thinning and expansion of the substorm plasma sheet, *J. Geophys. Res.*, *97*, 17,173–17,175, doi:10.1029/92JA01519.

Baumjohann, W., M. Hesse, S. Kokubun, T. Mukai, T. Nagai, and A. A. Petrukovich (1999), Substorm dipolarization and recovery, *J. Geophys. Res.*, *104*, 24,995–25,000, doi:10.1029/1999JA900282.

Birn, J. (2005), Three-dimensional magnetotail equilibria with prescribed boundary shapes, *J. Geophys. Res.*, *110*, A07203, doi:10.1029/2004JA010869.

Birn, J., M. Hesse, G. Haerendel, W. Baumjohann, and K. Shiokawa (1999), Flow braking and the substorm current wedge, *J. Geophys. Res.*, *104*, 19,895–19,904, doi:10.1029/1999JA900173.

Birn, J., J. Raeder, Y. Wang, R. Wolf, and M. Hesse (2004), On the propagation of bubbles in the geomagnetic tail, *Ann. Geophys.*, *22*, 1773–1786.

Bowling, S. B., and C. T. Russell (1976), The position and shape of the neutral sheet at 30-Earth radii distance, *J. Geophys. Res.*, *81*, 270–272, doi:10.1029/JA081i001p00270.

Chen, C. X., and R. A. Wolf (1993), Interpretation of high-speed flows in the plasma sheet, *J. Geophys. Res.*, *98*, 21,409–21,419, doi:10.1029/93JA02080.

Chen, C. X., and R. A. Wolf (1999), Theory of thin-filament motion in Earth's magnetotail and its application to bursty bulk flows, *J. Geophys. Res.*, *104*, 14,613–14,626, doi:10.1029/1999JA900005.

El-Alaoui, M. (2001), Current disruption during November 24, 1996, substorm, *J. Geophys. Res.*, *106*, 6229–6246, doi:10.1029/1999JA000260.

El-Alaoui, M., M. Ashour-Abdalla, R. J. Walker, V. Peroomian, R. L. Richard, V. Angelopoulos, and A. Runov (2009), Substorm evolution as revealed by THEMIS satellites and a global MHD simulation, *J. Geophys. Res.*, *114*, A08221, doi:10.1029/2009JA014133.

Goertz, C. K., and W. Baumjohann (1991), On the thermodynamics of the plasma sheet, *J. Geophys. Res.*, *96*, 20,991–20,998.

Harris, E. G. (1962), On a plasma sheet separating regions of oppositely directed magnetic field, *Nuovo Cimento*, *23*, 115–121.

Hayakawa, H., A. Nishida, E. W. Hones Jr., and S. J. Bame (1982), Statistical characteristics of plasma flow in the magnetotail, *J. Geophys. Res.*, *87*, 277–283.

Kaufmann, R. L., and W. R. Paterson (2008), Ion heat flux and energy transport near the magnetotail neutral sheet, *J. Geophys. Res.*, *113*, A05207, doi:10.1029/2007JA012929.

Kaufmann, R. L., W. R. Paterson, and L. A. Frank (2005), Relationships between the ion flow speed, magnetic flux transport rate, and other plasma sheet parameters, *J. Geophys. Res.*, *110*, A09216, doi:10.1029/2005JA011068.

Keika, K., et al. (2009), Observations of plasma vortices in the vicinity of flow-braking: A case study, *Ann. Geophys.*, *27*, 3009–3017.

Keiling, A., et al. (2009), Substorm current wedge driven by plasma flow vortices: THEMIS observations, *J. Geophys. Res.*, *114*, A00C22, doi:10.1029/2009JA014114.

Kistler, L. M., E. Moebius, W. Baumjohann, G. Paschmann, and D. C. Hamilton (1992), Pressure changes in the plasma sheet during substorm injections, *J. Geophys. Res.*, *97*, 2973–2983, doi:10.1029/91JA02802.

Kubyshkina, M., V. Sergeev, N. Tsyganenko, V. Angelopoulos, A. Runov, H. Singer, K. H. Glassmeier, H. U. Auster, and W. Baumjohann (2009), Toward adapted time-dependent magnetospheric models: A simple approach based on tuning the standard model, *J. Geophys. Res.*, *114*, A00C21, doi:10.1029/2008JA013547.

Lui, A. T. Y., A. Mankofsky, C.-L. Chang, K. Papadopoulos, and C. S. Wu (1990), A current disruption mechanism in the neutral sheet: A possible trigger for substorm expansions, *Geophys. Res. Lett.*, *17*, 745–748, doi:10.1029/GL017i006p00745.

McComas, D. J., S. J. Bame, C. T. Russell, and R. C. Elphic (1986), The near-Earth cross-tail current sheet: Detailed ISEE 1 and 2 case studies, *J. Geophys. Res.*, *91*, 4287–4301, doi:10.1029/JA091iA04p04287.

McFadden, J. P., C. W. Carlson, D. Larson, V. Angelopoulos, M. Ludlam, R. Abiad, B. Elliot, P. Turin, and M. Marckwordt (2008), The THEMIS ESA plasma instrument and in-flight calibration, *Space Sci. Rev.*, *141*, 277–302.

McPherron, R. L., A. Nishida, and C. T. Russell (1987), Is near-Earth current sheet thinning the cause of auroral substorm onset?, in *Quantitative Modeling of Magnetosphere-Ionosphere Coupling Processes*, edited by Y. Kamide and R. A. Wolf, p. 252, Kyoto Sangyo Univ., Kyoto, Japan.

Nakamura, R., D. N. Baker, D. H. Fairfield, D. G. Mitchell, R. L. McPherron, and E. W. Hones Jr. (1994), Plasma flow and magnetic field characteristics near the midtail neutral sheet, *J. Geophys. Res.*, *99*, 23,591–23,601.

Nakamura, R., et al. (2002a), Motion of the dipolarization front during a flow burst event observed by Cluster, *Geophys. Res. Lett.*, *29*(20), 1942.

Nakamura, R., et al. (2002b), Fast flow during current sheet thinning, *Geophys. Res. Lett.*, *29*(23), 2140, doi:10.1029/2002GL016200.

Nakamura, R., et al. (2004), Spatial scale of high-speed flows in the plasma sheet observed by Cluster, *Geophys. Res. Lett.*, *31*, L09804, doi:10.1029/2004GL019558.

Ohtani, S., H. J. Singer, and T. Mukai (2006), Effects of the fast plasma sheet flow on the geosynchronous magnetic configuration: Geotail and GOES coordinated study, *J. Geophys. Res.*, *111*, A01204, doi:10.1029/2005JA011383.

Ohtani, S., Y. Miyashita, H. Singer, and T. Mukai (2009), Tailward flows with positive B Z in the near-Earth plasma sheet, *J. Geophys. Res.*, *114*, A06218, doi:10.1029/2009JA014159.

Petrukovich, A. A., W. Baumjohann, R. Nakamura, A. Balogh, T. Mukai, K.-H. Glassmeier, H. Reme, and B. Klecker (2003), Plasma sheet structure during strongly northward IMF, *J. Geophys. Res.*, *108*(A6), 1258, doi:10.1029/2002JA009738.

Petrukovich, A. A., W. Baumjohann, R. Nakamura, A. Runov, A. Balogh, and H. Rème (2007), Thinning and stretching of the plasma sheet, *J. Geophys. Res.*, *112*, A10213, doi:10.1029/2007JA012349.

Rostoker, G. (1996), Phenomenology and physics of magnetospheric substorms, *J. Geophys. Res.*, *101*, 12,955–12,974, doi:10.1029/96JA00127.

Runov, A., et al. (2005a), Electric current and magnetic field geometry in flapping magnetotail current sheets, *Ann. Geophys.*, *23*, 1391–1403.

Runov, A., et al. (2005b), Reconstruction of the magnetotail current sheet structure using multi-point Cluster measurements, *Planet. Space Sci.*, *53*, 237–243, doi:10.1016/j.pss.2004.09.049.

Runov, A., V. Angelopoulos, V. A. Sergeev, K.-H. Glassmeier, U. Auster, J. McFadden, D. Larson, and I. Mann (2009), Global properties of magnetotail current sheet flapping: THEMIS perspectives, *Ann. Geophys.*, *27*, 319–328.

Sanny, J., R. L. McPherron, C. T. Russell, D. N. Baker, T. I. Pulkkinen, and A. Nishida (1994), Growth-phase thinning of the near-Earth current sheet during the CDAW 6 substorm, *J. Geophys. Res.*, *99*, 5805–5816, doi:10.1029/93JA03235.

Schindler, K., and J. Birn (1993), On the cause of thin current sheets in the near-Earth magnetotail and their possible significance for magnetospheric substorms, *J. Geophys. Res.*, *98*, 15,477–15,485, doi:10.1029/93JA01047.

Schödel, R., W. Baumjohann, R. Nakamura, V. A. Sergeev, and T. Mukai (2001a), Rapid flux transport in the central plasma sheet, *J. Geophys. Res.*, *106*, 301–314, doi:10.1029/2000JA900139.

Schödel, R., R. Nakamura, W. Baumjohann, and T. Mukai (2001b), Rapid flux transport and plasma sheet reconfiguration, *J. Geophys. Res.*, *106*, 8381–8390, doi:10.1029/2000JA900159.

Sergeev, V. A., D. G. Mitchell, C. T. Russell, and D. J. Williams (1993), Structure of the tail plasma/current sheet at 11 Re and its changes in the course of a substorm, *J. Geophys. Res.*, *98*, 17,345–17,366, doi:10.1029/93JA01151.

Sergeev, V. A., V. Angelopoulos, J. T. Gosling, C. A. Cattell, and C. T. Russell (1996), Detection of localized, plasma-depleted flux tubes or bubbles in the midtail plasma sheet, *J. Geophys. Res.*, *101*, 10,817–10,826, doi:10.1029/96JA00460.

Sergeev, V., V. Angelopoulos, C. Carlson, and P. Sutcliffe (1998), Current sheet measurements within a flapping plasma sheet, *J. Geophys. Res.*, *103*, 9177–9188, doi:10.1029/97JA02093.

Snekvik, K., et al. (2007), Cluster observations of a field aligned current at the dawn flank of a bursty bulk flow, *Ann. Geophys.*, *25*, 1405–1415.

Spence, H. E., and M. G. Kivelson (1990), The variation of the plasma sheet polytropic index along the midnight meridian in a finite width magnetotail, *Geophys. Res. Lett.*, *17*, 591–594, doi:10.1029/GL017i005p00591.

Takada, T., et al. (2006), Do BBFs contribute to inner magnetosphere dipolarizations: Concurrent Cluster and Double Star observations, *Geophys. Res. Lett.*, *33*, L21109, doi:10.1029/2006GL027440.

Thompson, S. M., M. G. Kivelson, K. K. Khurana, R. L. McPherron, J. M. Weygand, A. Balogh, H. Réme, and L. M. Kistler (2005), Dynamic Harris current sheet thickness from Cluster current density and plasma measurements, *J. Geophys. Res.*, *110*, A02212, doi:10.1029/2004JA010714.

Tsyganenko, N. A., and T. Mukai (2003), Tail plasma sheet models derived from Geotail particle data, *J. Geophys. Res.*, *108*(A3), 1136, doi:10.1029/2002JA009707.

Tsyganenko, N. A., and D. P. Stern (1996), Modeling the global magnetic field of the large-scale Birkeland current systems, *J. Geophys. Res.*, *101*, 27,187–27,198, doi:10.1029/96JA02735.

Ugai, M. (2009a), Fast reconnection evolution in an arcadelike magnetic loop structure, *Phys. Plasmas*, *16*(6), 062312, doi:10.1063/1.3158949.

Ugai, M. (2009b), Impulsive magnetic pulsations and electrojets in the loop footpoint driven by the fast reconnection jet, *Phys. Plasmas*, *16*(11), 112902, doi:10.1063/1.3267869.

Walsh, A. P., et al. (2009), Cluster and Double Star multipoint observations of a plasma bubble, *Ann. Geophys.*, *27*, 725–743.

Zhou, X.-Y., C. T. Russell, and D. G. Mitchell (1997), Three spacecraft observations of the geomagnetic tail during moderately disturbed conditions: Global perspective, *J. Geophys. Res.*, *102*, 14,425–14,438, doi:10.1029/97JA00683.

V. Angelopoulos, Institute of Geophysics and Planetary Physics, University of California, Los Angeles, CA 90095, USA.

W. Baumjohann, R. Nakamura, E. V. Panov, A. Retinò, and M. Volwerk, Space Research Institute, Austrian Academy of Sciences, Schmiedlstraße 6, A-8042 Graz, Austria. (evgeny_panov@mail.ru)

K.-H. Glassmeier, Institut für Geophysik und Extraterrestrische Physik, Technische Universitt Braunschweig, Mendelssohnstr. 3, D-38106, Braunschweig, Germany.

D. Larson and J. P. McFadden, Space Science Laboratory, University of California, Berkeley, CA 94720, USA.

A. A. Petrukovich, Space Research Institute of Russian Academy of Sciences, 84/32 Profsoyuznaya Str., 117997, Moscow, Russia.

V. A. Sergeev, Institute of Physics, Saint Petersburg State University, Saint Petersburg, 199034, Russia.

T. Takada, Institute of Space and Astronautical Science, 3-1-1 Yoshinodai, Sagamihara, Kanagawa 229-8510, Japan.